Published in final edited form as:
Science. 2009 March 27; 323(5922): 1743–1747. doi:10.1126/science.1167525.

Quantitative 3D Video Microscopy of HIV Transfer Across T Cell Virological Synapses

Wolfgang Hübner[1], **Gregory P. McNerney**[3], **Ping Chen**[1], **Benjamin M. Dale**[1], **Ronald E. Gordon**[2], **Frank Y. S. Chuang**[3], **Xiao-Dong Li**[4], **David M. Asmuth**[4], **Thomas Huser**[3,4], and **Benjamin K. Chen**[1,*]

[1]Division of Infectious Diseases, Department of Medicine, Immunology Institute, Mount Sinai School of Medicine, New York, NY 10029, USA

[2]Department of Pathology, Mount Sinai School of Medicine, New York, NY 10029, USA

[3]NSF Center for Biophotonics Science and Technology, University of California Davis (UCD), Sacramento, CA 95817, USA

[4]Department of Internal Medicine, University of California Davis Medical Center, Sacramento, CA 95817, USA

Abstract

The spread of HIV between immune cells is greatly enhanced by cell-cell adhesions called virological synapses, although the underlying mechanisms have been unclear. With use of an infectious, fluorescent clone of HIV, we tracked the movement of Gag in live CD4 T cells and captured the direct translocation of HIV across the virological synapse. Quantitative, high-speed three-dimensional (3D) video microscopy revealed the rapid formation of micrometer-sized "buttons" containing oligomerized viral Gag protein. Electron microscopy showed that these buttons were packed with budding viral crescents. Viral transfer events were observed to form virus-laden internal compartments within target cells. Continuous time-lapse monitoring showed preferential infection through synapses. Thus, HIV dissemination may be enhanced by virological synapse-mediated cell adhesion coupled to viral endocytosis.

Human immunodeficiency virus (HIV) infection leads to depletion of CD4 T cells throughout the lymphoid system. Both cell-free and cell-associated infection routes contribute to viral dissemination in vivo (1). In vitro, infection with cell-associated HIV can be thousands fold more efficient than infection with cell-free virus (2), and inhibition of cell-cell contacts severely limits replication (3). Infection through synapses between virus-carrying dendritic cells and CD4 T cells is highly efficient (4,5). For human T cell lymphotropic virus type I, viral synapses between T cells are essential for dissemination (6). For HIV, infected and uninfected CD4 T cells form virological synapses that organize viral receptors CD4, CXCR4, and Env (7). These infectious contacts are regulated by cell adhesion through integrins and intercellular adhesion molecules (8), dynamic actin and tubulin (9), cell signaling (10), and lipid raft recruitment (11). T cell virological synapses transfer virus with high efficiency (12), yet how this route fundamentally differs from cell-free infection remains unclear.

To examine the spatial and temporal organization of synapse formation, we used an infectious, fluorescent HIV clone, carrying a Gag-internal, interdomain insertion of the green fluorescent

*To whom correspondence should be addressed. ben.chen@mssm.edu.

Supporting Online Material: www.sciencemag.org/cgi/content/full/323/5922/1743/DC1

protein (GFP), called HIV Gag-iGFP (13). This virus faithfully reveals Gag localization, allowing infected cells and viral particles to be tracked with high sensitivity (12). Time-lapse fluorescence microscopy of virological synapse formation showed that 24% of HIV Gag-iGFP–expressing Jurkat cells formed stable adhesions to primary CD4 T cells within 4 hours (Fig. 1 and table S1A). After adhesion, 80% formed focal Gag accumulations at the contact site with an average 82-min interval (Fig. 1, A and B). In contrast, an Env-deficient clone was unable to induce cell-cell conjugates or Gag accumulation (table S1B), illustrating that adhesion precedes Gag redistribution.

In fixed samples, high-resolution confocal imaging revealed prominent Gag accumulations at the synapse (Fig. 1C). In three-dimensional (3D) reconstructions, these appeared as button-shaped discs, 1 to 3 mm in diameter (Fig. 1D and movie S1). Synaptic buttons were also observed in HIV Gag-iGFP–expressing primary CD4 T cells cocultured with homologous primary CD4 cells (fig. S1). We assessed viral assembly at the synapse by measuring Gag oligomerization with fluorescence resonance energy transfer (FRET) (13–15) between Cerulean and Venus variants of HIV Gag-iGFP, which form a donor-acceptor FRET pair (16). Excitation of the Cerulean donor in cotransfected Jurkat cells generated a robust Venus-shifted FRET signal at synaptic buttons that is indicative of Gag homo-oligomerization (Fig. 1E). Photobleaching the Venus acceptor at a synapse lead to increased donor emission, providing additional evidence for FRET (Fig. 1, F to H, and fig. S2). Three-dimensional reconstruction of FRET images revealed concentrated Gag oligomerization at synapses (movie S2).

With transmission electron microscopy, we observed that 100-nm budding viral crescents at the virological synapse protruded from the donor cell with bud tips directly abutting the target cell membrane (Fig. 1I). Viral buds were also observed far from the synapse, although at lower densities (fig. S3). Native, non–GFP-expressing HIV induced similar budding crescents, ruling out that GFP induced these accumulations (fig. S4). In thick 150-nm sections, near-complete viral buds and a virus-containing invagination in the synapsed target cell were observed (fig. S4, A and B).

To capture the dynamics of Gag trafficking, reorganization, and viral transfer with higher temporal and spatial resolution, we recorded highspeed, spinning disc confocal fluorescence images. Forty-three putative synaptic events encompassing 1187 min revealed dynamic Gag movements during virological synapse formation (table S2). New synaptic button formation ($n = 4$) was captured where patches of membrane-associated Gag moved toward the cell adhesion site within minutes (Fig. 2A and movie S3). At existing buttons, a ring-shaped zone of Gag depletion often surrounded the synaptic button (Fig. 2B), indicative of a synapse-proximal region from which Gag was recruited.

HIV Gag-iGFP–labeled structures ($n = 8$) close to existing buttons moved rapidly and directionally into the button (Fig. 2C, fig. S5, and movies S4 to S6). The structures moved into the synapse with average velocities of 0.10 to 0.25 mm/s and peaks up to 0.8 mm/s (Fig. 2C and fig. S5). Other small, mobile Gag puncta emerged from and then moved back into the synaptic button (Fig. 2D and movie S7). The fast, directional movement of Gag was seen predominantly from nearby puncta.

During cell-to-cell viral transfer ($n = 10$, table S2), fluorescent Gag signal protruded from buttons, penetrated the attached target cell, was released into the target cell, and then migrated distally with a mean velocity of 0.12 μm/s (Fig. 2E and movie S8). Notably, puncta 1.5 μm in diameter were observed (fig. S6A), and on occasion an entire synaptic button was transferred (movie S9). Large vesicular structures were also observed to fractionate into smaller vesicles while moving toward the distal pole of the cell (movies S4 and S8). The size of these

translocated puncta exceeds individual clathrin- or caveolin-associated structures, which are uniformly small (100 to 200 nm) (17). By using quantitative confocal microscopy, we found that the accumulation and maintenance of Gag puncta in target cells was remarkably stable over time (fig. S6, B to D, and movie S10).

The GFP signal in flow-sorted HIV+ CD4 target cells was uniformly punctate, without evidence of syncitia, and confocal imaging suggested that puncta were not surface-associated (fig. S7). Anti-Env staining of the Gag-iGFP puncta required cell permeabilization, indicating that Env was present in an internal Gag+ compartment (Fig. 2, F and G). Transmission electron microscopy of the target cells revealed multivesicular structures, which were not seen in control, unexposed cells, that contained viruslike densities inside 1- to 2-mm compartments (Fig. 2H). We conclude that synapses target HIV into vesicular compartments within recipient cells.

To track the fate of cells after synapse formation, we performed continuous, long-duration imaging. Jurkat donor cells were cotransfected with HIV Gag-iGFP and HIV NL-GI, an HIV molecular clone that expresses GFP in place of the viral early gene nef (18). This approach can visualize viral transfer (as puncta), as well as productive infection (as diffuse GFP) in the target cell. In example one, the infected cell synapsed with the target cell for 18 hours, the cells separated, and at 32 hours a diffuse, bright GFP signal indicated productive infection (Fig. 3, A C, and movie S11). Bystander target cells remained negative. Over 67 hours, 112 conjugates tracked resulted in seven productively infected MT4 target cells (table S3). In five cases, synapses were observed, and in four cases virus transfer was recorded (Fig. 3, A to C, and movie S12). Under culture conditions that limited new cell-cell interactions, productively infected cells arose preferentially after observed virological synapse events.

Because synapse-mediated viral transfer is coreceptor-independent (12,19), we tested whether infection through T cell synapses requires coreceptor expression. Infection of MT4 cells by cell-associated HIV was inhibited when cells were separated by a 0.4-μm transwell barrier (Fig. 4A). Under these contact-dependent infection conditions, productive infection by cell-associated HIV NL-GI was inhibited by CXCR4-antagonist, AMD3100 (Fig. 4B). Furthermore, productive infection by cell-associated R5-tropic virus HIV NL-GI (JRFL) was dependent on expression of the chemokine receptor, CCR5 (Fig. 4C). The results suggest that infection through T cell synapses does not bypass the coreceptor requirement.

Synapse-mediated viral transfer is potently inhibited by actin inhibitors such as cytochalasin D (9,12). We find that cytochalasin D had little effect on cell-free HIV infection yet effectively inhibited productive infection by cell-associated HIV (Fig. 4D). Additionally, a well-characterized patient antisera, which can potently block cell-free infection but not transfer of virus through virological synapses (12), did not efficiently block infection of the homologous cell-associated virus (Fig. 4E). Thus, inhibitor studies clearly distinguish the mechanisms of cell-free from those of cell-associated infection.

The live imaging of HIV cell-to-cell transfer reveals that dynamic Gag movements in infected cells organize Gag puncta into synaptic buttons from which HIV is directly transferred into adjacent target cells. Although endocytic entry of cell-free HIV contributes only modestly to productive infection (20–22), our results suggest that the cell-to-cell transmission could favor endocytic routes. Thus when spreading via synapses, it is possible that HIV resembles a majority of viruses that enter preferentially through endocytosis (e.g., influenza, adenoviruses, picornaviruses, alphaviruses) (23). Given this scenario, the tight coupling of Env fusogenicity with particle maturation (24,25) may activate viral fusion within a target cell compartment that is cloistered from neutralizing antibodies (12). Alternatively, the prominent endocytic process that accompanies synapse formation may create viral reservoirs in intracellular compartments.

Future vaccine strategies may be focused against unique cell-surface Env epitopes that block cell-associated infection, and future antiviral drugs may target factors required for synapse formation. Ultimately the dynamics of virological synapse formation must be understood within lymphoid tissues, where high density and lymphocyte mobility (26) are likely to promote synaptic viral spread.

Supplementary Material

Refer to Web version on PubMed Central for supplementary material.

Acknowledgments

We thank R. H. Cheng, V. Simon, M. Klotman, R. Iyengar, and A. Del Portillo for critiques and discussions; R. Huq for microscopy support; S. Izadmehr for image analysis; M. Grisotto and V. Sahi for cell sorting; H. Bell for electron microscopy support; and S. Lira for imaging support. Work was supported by NIH grant AI074420-02, Burroughs Wellcome Fund Investigator Award, and Hirschl Weill-Caulier Career Scientist Award to B.K.C. Imaging was supported by Mount Sinai School of Medicine–Microscopy Shared Resource Facility grants NIH-NCI 5R24 CA095823-04, NSF-DBI-9724504, and NIH-S10RR09145-01; by the NSF Center for Biophotonics Science and Technology (cooperative agreement PHY012099); a UCD Health System Research Award to T.H.; and the UCD Clinical and Translational Science Center grant NIH-NCRR ULRR024146 (T.H. and D.M.A.).

References and Notes

1. Haase AT. Nat Rev Immunol 2005;5:783. [PubMed: 16200081]
2. Dimitrov DS, et al. J Virol 1993;67:2182. [PubMed: 8445728]
3. Sourisseau M, Sol-Foulon N, Porrot F, Blanchet F, Schwartz O. J Virol 2007;81:1000. [PubMed: 17079292]
4. Cameron PU, et al. Science 1992;257:383. [PubMed: 1352913]
5. McDonald D, et al. Science 2003;300:1295.10.1126/science.1084238 [PubMed: 12730499]published online 1 May 2003
6. Igakura T, et al. Science 2003;299:1713.10.1126/science.1080115 [PubMed: 12589003]published online 13 February 2003
7. Jolly C, Kashefi K, Hollinshead M, Sattentau QJ. J Exp Med 2004;199:283. [PubMed: 14734528]
8. Jolly C, Mitar I, Sattentau QJ. J Virol 2007;81:13916. [PubMed: 17913807]
9. Jolly C, Mitar I, Sattentau QJ. J Virol 2007;81:5547. [PubMed: 17360745]
10. Sol-Foulon N, et al. EMBO J 2007;26:516. [PubMed: 17215865]
11. Jolly C, Sattentau QJ. J Virol 2005;79:12088. [PubMed: 16140785]
12. Chen P, Hubner W, Spinelli MA, Chen BK. J Virol 2007;81:12582. [PubMed: 17728240]
13. Hubner W, et al. J Virol 2007;81:12596. [PubMed: 17728233]
14. Derdowski A, Ding L, Spearman P. J Virol 2004;78:1230. [PubMed: 14722278]
15. Larson DR, Ma YM, Vogt VM, Webb WW. J Cell Biol 2003;162:1233. [PubMed: 14517204]
16. Rizzo MA, Springer GH, Granada B, Piston DW. Nat Biotechnol 2004;22:445. [PubMed: 14990965]
17. Lakadamyali M, Rust MJ, Zhuang X. Cell 2006;124:997. [PubMed: 16530046]
18. Cohen GB, et al. Immunity 1999;10:661. [PubMed: 10403641]
19. Blanco J, et al. J Biol Chem 2004;279:51305. [PubMed: 15371410]
20. Fackler OT, Peterlin BM. Curr Biol 2000;10:1005. [PubMed: 10985390]
21. Marechal V, et al. J Virol 2001;75:11166. [PubMed: 11602756]
22. Schaeffer E, Soros VB, Greene WC. J Virol 2004;78:1375. [PubMed: 14722292]
23. Marsh M, Helenius A. Cell 2006;124:729. [PubMed: 16497584]
24. Wyma DJ, et al. J Virol 2004;78:3429. [PubMed: 15016865]
25. Wyss S, et al. J Virol 2005;79:12231. [PubMed: 16160149]
26. Germain RN, Miller MJ, Dustin ML, Nussenzweig MC. Nat Rev Immunol 2006;6:497. [PubMed: 16799470]

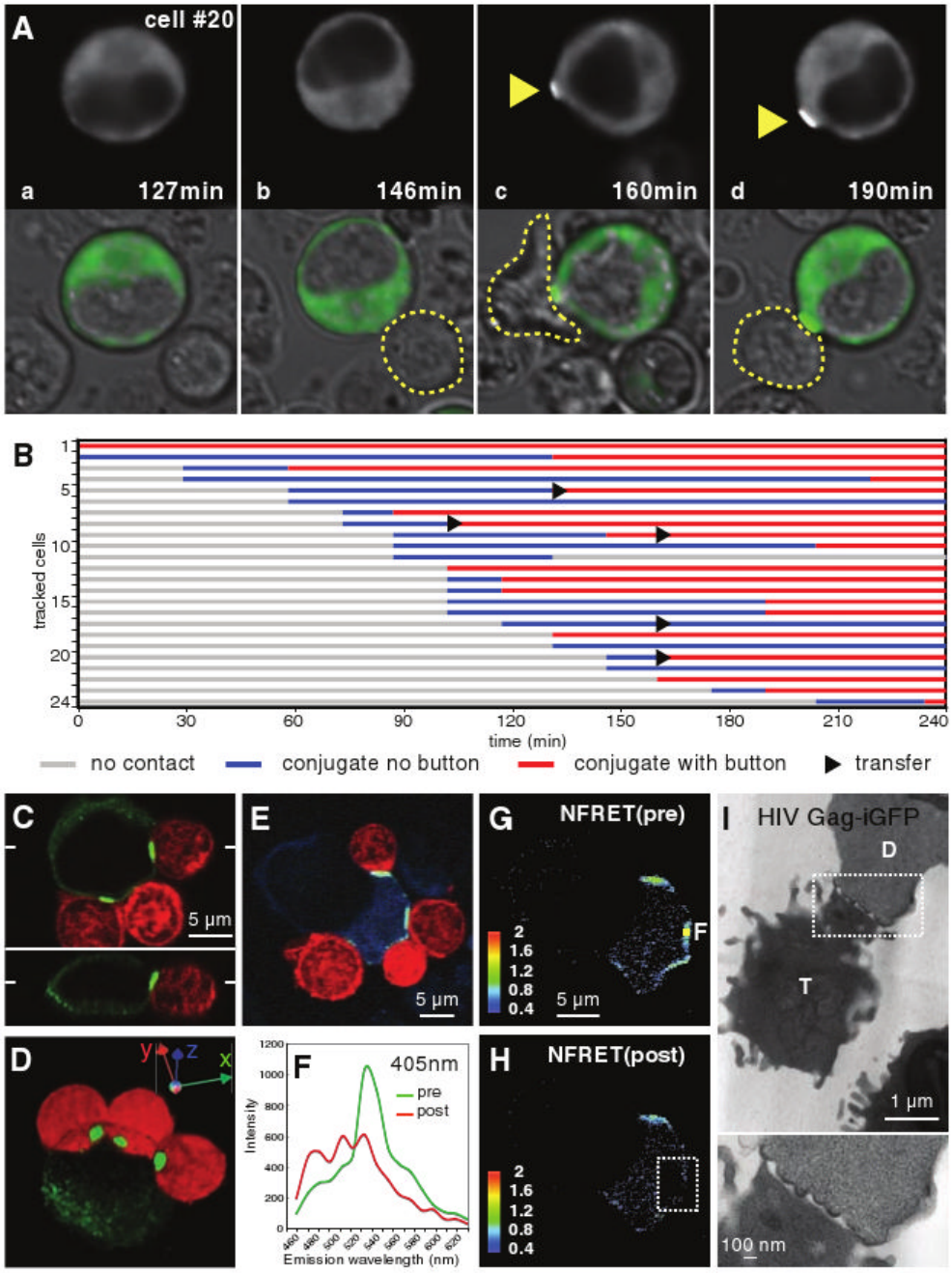

Fig. 1.

Gag accumulates at synaptic buttons after T cell adhesion. (**A**) Time-lapse fluorescence imaging of synapse formation between an HIV Gag-iGFP–expressing Jurkat cell and a CD4 T cell. GFP image (top) and GFP/phase contrast overlay (bottom). Cells (a) before stable contact, (b) in stable adhesion (outlined), and (c and d) showing synaptic buttons (arrowheads). (**B**) Timing of synapse formation following 24 HIV+ Jurkat cells; each line represents an interactive cell. (**C**) Confocal fluorescence image of an HIV Gag-iGFP-expressing Jurkat T cell (green) synapsed with three primary CD4 T cells [red, labeled with CellTracker Orange CMRA (Invitrogen, Carlsbad, CA)]. Positioning of perpendicular planes marked at edges. (**D**) Reconstructed 3D view of (C). (**E** to **H**) FRET analysis of Gag-iCerulean (donor) and Gag-

iVenus (acceptor) fluorophores at the synaptic button. (**E**) Three-color overlay donor Cerulean (blue, 405-nm excitation), FRET channel (green, 405-nm excitation), and target cells [red, 543-nm excitation stained with CellTracker Orange CMTMR (Invitrogen)]. (F) Emission spectra at synaptic button, point F, pre- and postacceptor photobleaching. (G and H) Normalized FRET (NFRET) signal (13) before and after acceptor photobleaching in boxed area. (**I**) Transmission electron micrographs of the synaptic junction between HIV Gag-iGFP–expressing donor, D, and target, T, cells. Low (top) and high (bottom) magnification of 70-nm sections.

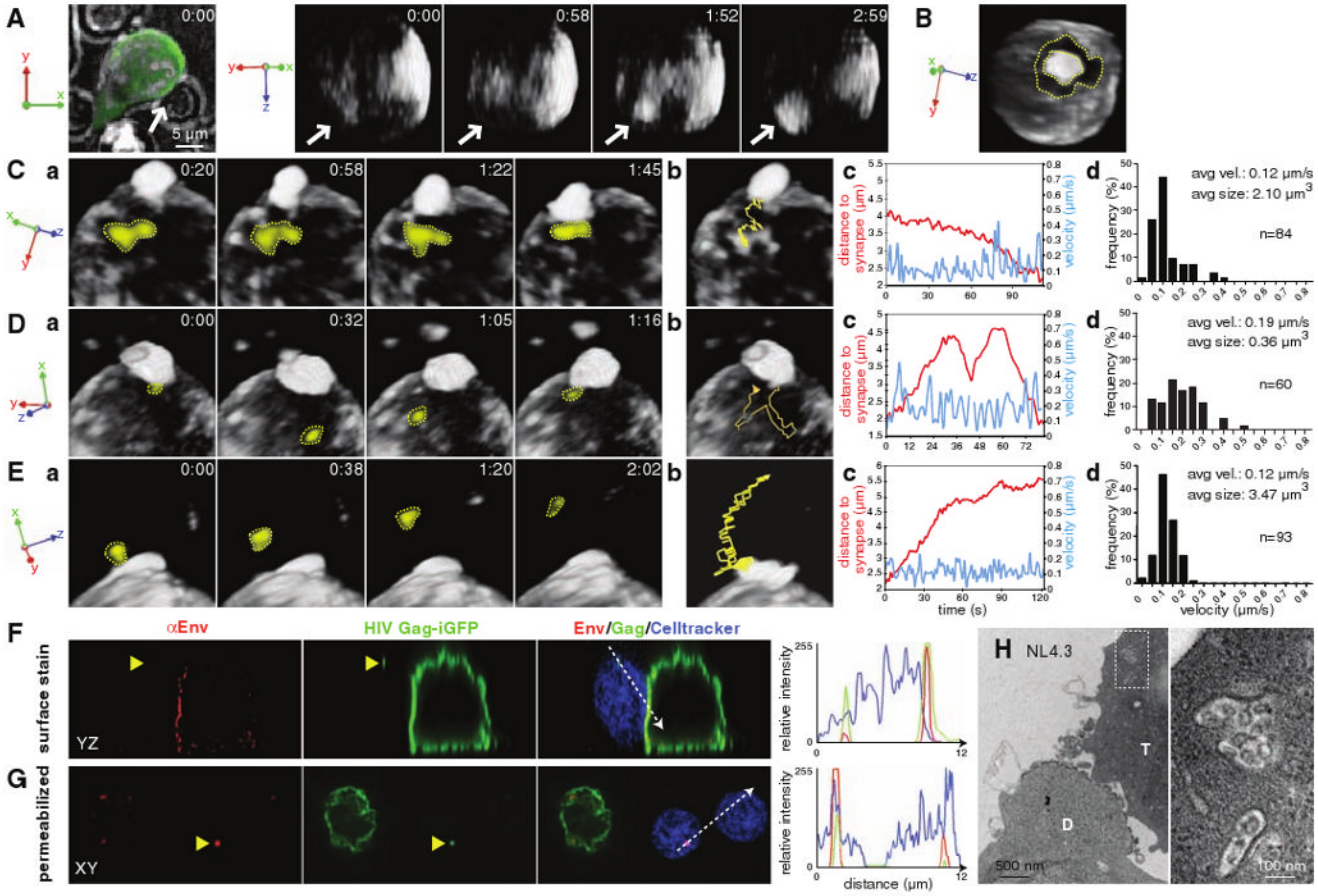

Fig. 2.

Dynamic recruitment of Gag puncta to the synapse and viral transfer into a target cell compartment revealed with rapid spinning-disc 3D confocal fluorescence microscopy. (**A**) Formation of a buttonlike accumulation of Gag at the site of adhesion, *z* projection at time = 0 (left), selected 3D reconstructions of contact site (arrows) over time (right four images). (**B**) A zone of Gag depletion, 2 to 3 μm wide, surrounds the synaptic button (dotted yellow line). (**C**) Patches of synapse-proximal Gag merge into the synapse. (**D**) A Gag-iGFP puncta moves out of and into the synapse. (**E**) During a transfer event, Gag puncta emerge from the synapse, separate, and then move to the distal pole. In (C) to (E), (a) selected frames highlight movement of Gag-iGFP puncta (yellow). (b) Object path is overlayed on the initial image. (c) Object distance to the synapse center and relative velocity are graphed over time. (d) Histogram distribution of the tracked objects velocities. (**F** and **G**) Immunostaining of Gag puncta requires membrane permeabilization. (F) Nonpermeabilized, anti-Env immunostain (red) does not stain the Gag-iGFP+ puncta (green) within the CD4 target cell (CellTracker Blue CMF2HC, Invitrogen), whereas surface Env-staining at synapse is observed. Three-color intensity profile along the 12-μm line (right). (G) Permeabilization of fixed cells reveals anti-Env immunostain (red) at the GFP puncta (green) within the CD4 target cell (blue). (**H**) Transmission electron micrograph of vesicles containing corelike structures in a CD4 cell engaged in synapse with an HIV-infected Jurkat cell. Low (left) and high (right) magnification of 70-nm sections.

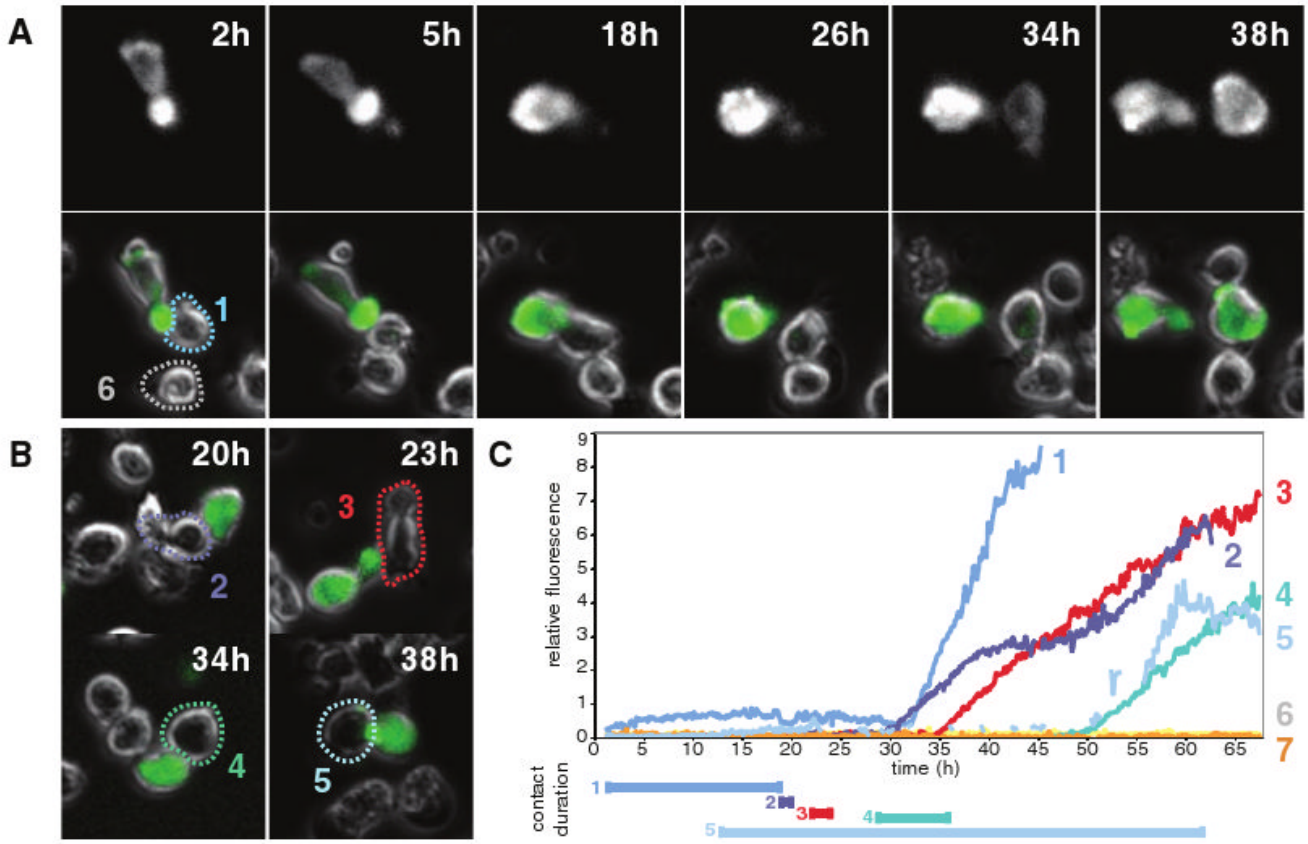

Fig. 3.

Productive infection of synapsed cells is visualized by 72-hour imaging of immobilized cells engaged in virological synapse. (**A**) Donor cells cotransfected with HIV Gag-iGFP to track viral transfer and HIV NL-GI to visualize new early gene expression in target cells. Images show a synapsed pair where the target cell (number 1) separates from donor at 18 hours and expresses increasing levels of diffuse GFP at 32 hours. Top row shows GFP images; bottom, GFP/phase overlays. (**B**) Four examples of synapsed MT4 target cells that subsequently expressed HIV (numbers 2 to 5). (**C**) Fluorescence intensity of the target cells 1 to 7. Numbers 6 and 7 are control bystander cells. Duration of cell contact indicated on bottom.

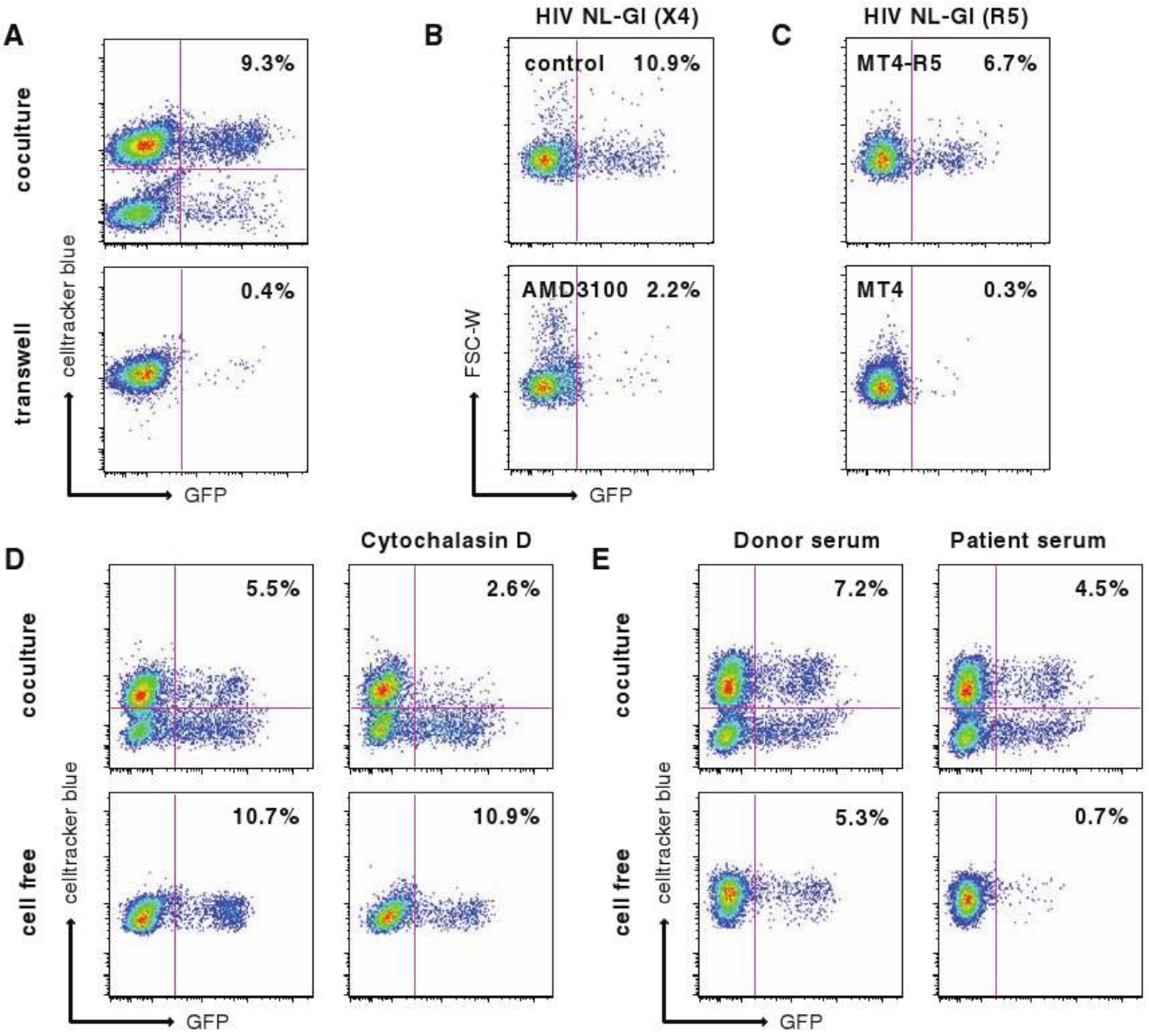

Fig. 4.

Cell-associated infection is coreceptor-dependent and actin-dependent and can resist a neutralizing antiserum. (**A**) HIV NL-GI–expressing Jurkat cells were cocultured with CellTracker Blue CMF2HC–labeled MT4 cells in the absence or the presence of a 0.4-μm transwell barrier between cells. Productive infection (GFP expression) in CellTracker-labeled target cells was measured by flow cytometry at 48 hours. (**B**) Coreceptor antagonist AMD3100 (10 μg/ml) inhibits infection of target cells by cell-associated X4-tropic virus, HIV NL-GI, at 48 hours. Productive infection in gated target cells indicated by GFP expression and is plotted against forward scatter width (FSC-W). (**C**) Cell-associated R5-tropic virus infects CCR5-expressing MT4 cells but not CCR5-negative MT4 cells. Jurkat cells expressing R5-tropic HIV NL-GI(JRFL) were donor cells. (**D**) Cytochalasin D (2.5 μM) inhibits cell-associated infection (top) but fails to block infection with cell-free virus (bottom). (**E**) A neutralizing antiserum that blocks cell-free infection (bottom) is less effective at blocking homologous cell-associated infection (top). Results representative of at least three independent experiments.